World Academy of Science, Engineering and Technology
International Journal of Aerospace and Mechanical Engineering
Vol:5, No:7, 2011

Numerical Investigation of a Slender Delta Wing in Combined Force-Pitch and Free-Roll

Yang Xiaoliang, Liu Wei, Wang Hongbo, and Zhao Yunfei

***Abstract*—**Numerical investigation of the characteristics of an 80° delta wing in combined force-pitch and free-roll is presented. The implicit, upwind, flux-difference splitting, finite volume scheme and the second-order-accurate finite difference scheme are employed to solve the flow governing equations and Euler rigid-body dynamics equations, respectively. The characteristics of the delta wing in combined free-roll and large amplitude force-pitch is obtained numerically and shows a well agreement with experimental data qualitatively. The motion in combined force-pitch and free-roll significantly reduces the lift force and transverse stabilities of the delta wing, which is closely related to the flying safety. Investigations on sensitive factors indicate that the roll-axis moment of inertia and the structural damping have great influence on the frequency and amplitude, respectively. Moreover, the turbulence model is considered as an influencing factor in the investigation.

***Keywords*—**combined force-pitch and free-roll, numerical simulation, sensitive factors, slender delta wing, wing rock

NOMENCLATURE

c	= root chord length
S	= wing area
ρ	= density
V	= velocity
q	= dynamic pressure, $0.5\rho_\infty V_\infty^2$
Ma	= Mach number
x,y,z	= Cartesian coordinates
ξ,η,ζ	= body-fitted coordinates
t	= time
Δt	= time step
Q	= conservative variables
E	= fluxes
σ	= incidence angle
θ	= pitching angle
ϕ	= rolling angle
ω	= angular velocity
k	= general variables; reduced frequency
u,v,w	= velocity component
C_l	= roll moment coefficient, $M_x/(q_\infty S_{ref} c)$
μ	= structural damping coefficient
I	= roll-axis moment of inertial
Subscripts	
∞	free stream
0	initial
ref	reference
v	viscid
x,y,z	corresponding axis component

This work is supported by the National Nature Science Foundation of China (No.90716015) and the National Basic Research program of China (No.2009CB723800).

Yang Xiaoliang is PH.D candidate with the Department of Aerospace and Engineering, National University of Defense and Technology, Changsha, Hunan, P.R.China (e-mail: china95189@yahoo.com.cn).

Liu Wei is the corresponding author and professor with the Department of Aerospace and Engineering, National University of Defense and Technology, Changsha, Hunan, P.R.China (phone: +86-731-84576137; fax: +86-731-84512301; e-mail: fishfather6525@sina.com).

Wang Hongbo is PH.D candidate with the Department of Aerospace and Engineering, National University of Defense and Technology, Changsha, Hunan, P.R.China.

Zhao Yunfei is PH.D candidate with the Department of Aerospace and Engineering, National University of Defense and Technology, Changsha, Hunan, P.R.China.

I. INTRODUCTION

ONE of the most common dynamic phenomena experienced by slender wing aircraft flying at high angles of attack is the one known as wing rock. Wing rock is a complicated motion that typically affects several degrees of freedom (DOF) simultaneously. As the name implies, however, the primary motion is an oscillation in roll [1]. As the delta wing is the main function plate of lift force and actual configuration of modern combat aircraft, the delta wings oscillating in roll at low speed regime have received a substantial volume of experimental [2]-[5] and computational [6]-[8] research work. It should be pointed out that wing rock is not only limited to a few aircraft but also a phenomenon which can be traced back to some of the early swept-wing fighter airplanes. In fact, over 13 modern aircrafts have been documented to exhibit this phenomenon [1]. For the sake of flying safety, a considerable quantity of programs have been promoted, such as, the Abrupt Wing Stall (AWS) program [9]-[11] sponsored by NASA Langley Research Center (LaRC) and U.S. Navy.

The concept of vortical lift force has made the delta wing the most popular configuration incorporated in modern combat aircraft. With the help of advance control systems, moreover, it becomes more and more feasible for combat aircraft to maneuver in high angle of attack. It is generally agreed that the lift force will be enforced when the aircraft experiences an upstroke in pitching. At high angle of attack, the high reduced frequency can effectively delay the vortex break and consequently delay the stall. A quantity of researches aiming at complicated aircraft or simple delta wing [12]-[14] confirmed this conclusion. However, the aircraft with highly swept platform is susceptible to oscillatory phenomenon during

excursions into the high angle of attack regime. The motion described above refers to force pitching and free rolling distinguished for the coupling effects and interactions in different DOF. The characteristics of aircraft in combined force-pitch and free-roll is different from both the free-to-roll motion in single DOF and the purely pitching motion in the meaning of dynamics and kinematics. A few researches attempt to address this coupling effect by purely forced motion in pitching and rolling [15], [16], however, the inherent limitation in methodology handicaps further results. Owing to the difficulties lying in experiment designing and measuring, only a few experimental efforts [17]-[20] are committed to this regime of motion of delta wing. To the author's knowledge, compared with the researches of single DOF wing rock, the numerical investigation about delta wing in this kind of double DOF motion is seldom addressed in published literature.

In this paper, the 80° sharp-edged delta wing is released to oscillate in roll around the body axis during forced pitching about a mean angle of incidence of 20° and a pitch axis at the half chord length. The amplitude and reduced frequency of the force pitching motion are 20°and 0.005, respectively. The focus of this work is to numerically simulate the double DOF motion of delta wing in force pitching and free rolling, analyzing the aerodynamic characteristics and orienting the sensitive factors that may influence the kinematics characteristics of the delta wing.

II. Numerical Approach

A. Flow Governing Equations

Equation Chapter 1 Section 1

The unsteady, three-dimensional, compressible, full Navier-Stokes equations in strongly conservative form have been used. The equations have been written in a fixed inertial frame of reference and transformed to the computational domain using a generalized time-dependent transformation (ξ,η,ζ,t). The dimensionless form is given as:

$$\frac{\partial Q}{\partial t}+\sum_k \frac{\partial E_k}{\partial k}=\sum_k \frac{\partial E_{vk}}{\partial k} \qquad k=\xi,\eta,\zeta \tag{1}$$

Where:

$$k=k(x,y,z,t) \tag{2}$$

$$Q=J^{-1}(\rho,\rho u,\rho v,\rho w,\rho e) \tag{3}$$

The definitions of the inviscid and viscid fluxes E_k and E_{vk} are detail in [21].

B. Rigid Body Dynamics Equations

The relevant DOF in this study are the pitching and rolling. The pitching movement is assigned by a force sinusoidal equation, while the rolling motion is governed by a rolling equation written in the body-axes frame of reference to keep the roll-axis moment of inertia constant throughout the entire motion.

The sinusoidal equation of pitching movement is given by:

$$\sigma=\sigma_0-\theta \quad , \quad \theta=-\theta_m\sin(kt) \tag{4}$$

The σ is the incidence angle. The θ is the pitching angle defined positive when the apex of the delta wing pitching downwards.

The rolling equation is a second-order autonomous ordinary differential equation in time and its nondimensional form is given as follow:

$$I_x\ddot{\phi}=C_{Mx}-\mu_x\dot{\phi} \tag{5}$$

The symbol ϕ is the rolling angle defined positive when the left-hand side (pilot view) of the wing moving downwards. The μ_x is the coefficient of structural damp. The C_{Mx} is a dimensionless coefficient, in which the rolling moment coefficient about the longitudinal axis, the non-dimension principal mass moment of inertial and the angular velocity are incorporated. It is described as:

$$C_{Mx}=C_l-(I_z-I_y)\omega_y\omega_z \tag{6}$$

C. Solution Algorithm

The implicit, finite volume scheme is used to solve the unsteady, three dimensional, compressible, full Navier-Stokes equations. The Nonoscillation, contains No free parameters and Dissipative (NND) flux-difference splitting scheme [22] is employed to discretize the inviscid fluxes, while the second-order accurate central difference scheme is applied to the discretization of the viscous fluxes which are linearized in time, eliminated in the implicit operator and retained in the explicit terms. In order to evaluate the influence of turbulence flow, the Spalart-Allmaras (SA) model is applied to some case of the investigation.

The Lower-Upper Symmetric Gauss-Seidel (LU-SGS) scheme is employed to enhance the efficiency of time integration, besides a dual-time-step method [23] which is a Newton-like sub-iteration process is employed to reduce the effect of the inherent time lag in applying the boundary conditions and reduce the factorization error for unsteady-state calculations.

A second-order-accurate finite difference scheme [8] is applied to discretize the rigid-body dynamics equation(5), given by:

$$\phi^{n+1}=k_1\phi^n+k_2\phi^{n-1}+k_3\phi^{n-2}+k_4 \tag{7}$$

Where:

$$k_1=\frac{10+4\Delta tc_2}{4+3\Delta tc_2},k_2=\frac{8+\Delta tc_2}{4+3\Delta tc_2}$$
$$k_3=\frac{2}{4+3\Delta tc_2},k_4=\frac{2\Delta t^2\bar{C}_{Mx}^{n+1}}{4+3\Delta tc_2} \tag{8}$$

D. Boundary Conditions

All boundary conditions are explicitly implemented, including far-field conditions, solid-boundary conditions and connecting conditions. At the far-field boundaries, the non-reflective boundary conditions based on Riemann-invarient are enforced. On the oscillating wing surface, the dynamic boundary condition $\frac{\partial p}{\partial n}=-\rho\cdot\vec{a}\cdot\vec{n}\,|_{wall}$ is employed as pressure condition and the adiabatic boundary condition as temperature condition.

III. Results and Discussions

In Fig.1, an O-H type grid is used to model the 80° swept-back, sharp-edged delta wing considered in this numerical investigation. The computational domain extends 2.5 chord lengths forward and 5 chord lengths backward from the wing tailing edge. The radius of the computational domain is 4 chord lengths. The minimum grid size in the normal direction to the wing surface is 1.0×10^{-4} chord length on the whole solid surface.

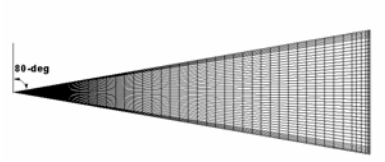

Fig. 1 80° delta wing model

A. The Characteristics of Single DOF wing rock

Considerable experimental and numerical researches aiming at predicting the self-excited oscillation of the 80° swept-back delta wing were conducted in the past several decades. These results are qualitatively consistent with each other, however, accompanied by discrepancies in the amplitude and frequency of oscillations. Various reasons, including the shape of leading edge, structural damping, etc. are directly responsible for these phenomena

In this section, the Single DOF self-excited rolling oscillation of the 80° swept-back, sharp-edged delta wing is predicted numerically in Fig.2. The initial condition corresponds to the solution of the wing held at 30° angle of attack and 0° roll angle at a Mach number and Reynolds number of 0.35 and 1.0×10^6, respectively. The wing is then released to respond to the fluid with the body-fixed x-axis moment of inertial, I_x=0.65. Fig.2 shows the time history and phase of the resultant motion. From 0°, the wing oscillates in roll with growing amplitude and periodicity is achieved 6 cycles later. By t=120, the motion is completely periodic with a maximum limit-cycle amplitude of 38.6°. This result agrees well with other predictions from experiment and computation.

B. The Characteristics of delta wing in combined force-pitch and free-roll

In this section, the characteristics of delta wing in combined force-pitch and free-roll are investigated with the same grid and the same free-stream conditions. The wing is forced to oscillate in pitching around an axis located at the half-chord length. The pitching motion is impulsively started from the mean incidence angle σ_0=20° , with an amplitude of θ_m=20° and a reduced frequency of k=0.005. About rolling, with the mass moment of inertial about the body-axis and roll damp of I_x=0.65 and μ_x=0.0, respectively, the wing is released to respond to the fluid during the forced pitching motion.

The double DOF motion of combined force-pitch and free-roll is numerically predicted as depicted in Fig.3. Due to the influence of dynamic incidence, the wing experiences a growing in amplitude and frequency of rolling motion in the upstroke pitching procession, after achieving the maximum amplitude around the peak of incidence angle the rolling amplitude and frequency of delta wing decrease with the declination of incidence angle. Although the free rolling frequency of delta wing around the crest region of incidence angle is nearly the same as that of self-excited wing rock in single DOF motion, it is extremely reduced in the trough region of incidence angle.

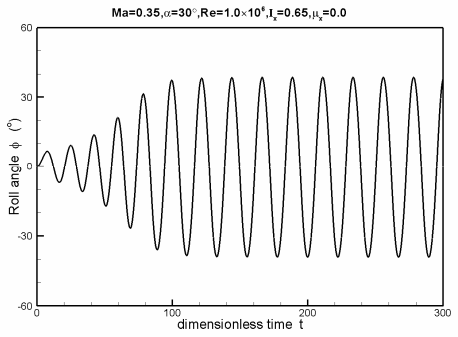

(a) Time history of roll angle

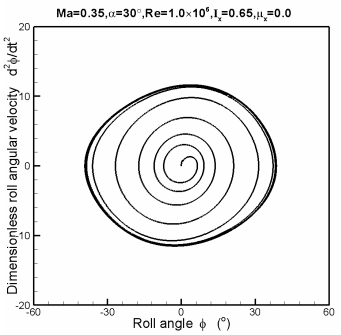

(b) Phase-curve

Fig. 2 Characteristics of Self-excited roll motion

The present computational roll-angle history exhibits a similar tendency with the experimental data [17] depicted in Fig.4. However, discrepancies in amplitude and frequency of rolling angle are also observed. Moreover, at the trough region of incidence angle of experiment, the rolling delta wing unexpectedly halts at -17° rolling angle for a considerably long time. The phenomenon in the experimental time history of rolling angle behaves as a plateau-curve which is not captured in the present calculation. This difference is usually attributed to the absence of friction generated by the bearing. However, further investigations in sensitive factors indicate that the reasons accounting for this phenomenon are going with multiple factors, such as moment of inertia and turbulence flow, which are to be documented later in part C.

Fig.5 shows a similarity between the phase curves obtained by the present calculation and that by experiment. The crossed

part of phase-curve indicates that the dynamic incidence has significant influence on the rolling movement.

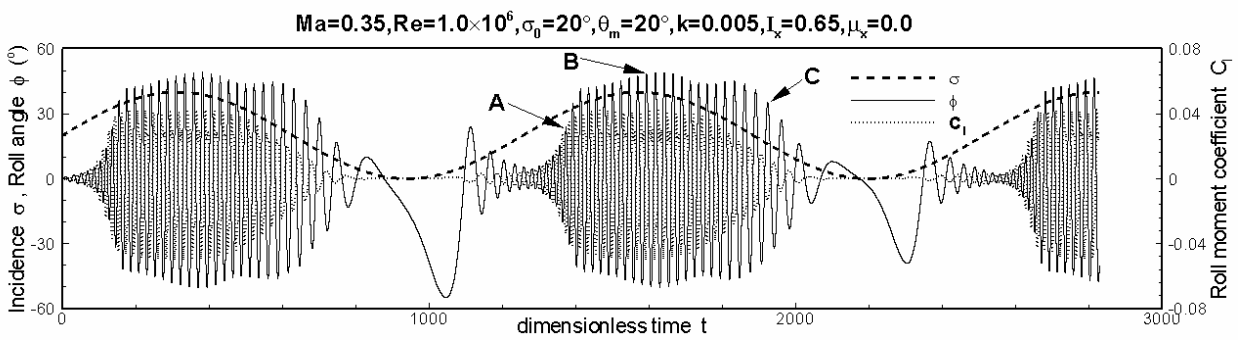

Fig. 3 Attitude angles and roll-moment coefficient versus time in combined force-pitch and free-roll motion

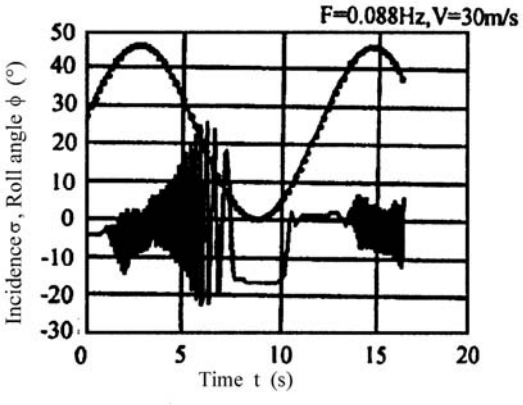

Fig. 4 Experimental history of rolling angle and incidence [17]

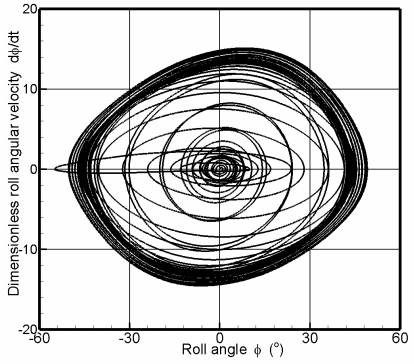

(a) Calculation

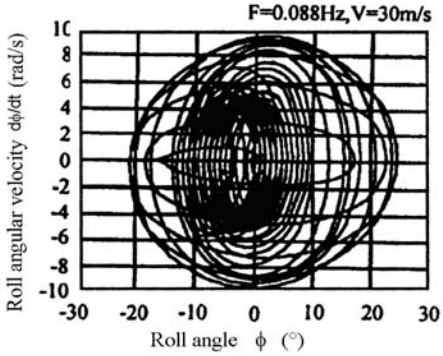

(b) Experiment [17]

Fig. 5 Phase-curve of combined force-pitch and free-roll motion

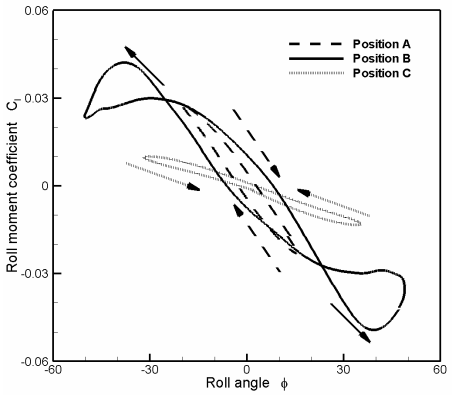

Fig.6 Hysteresis loops of roll-moment coefficient

In Fig.3, there are three positions denoted by A, B and C, representing the augmentation, maintenance and attenuation of the amplitude of rolling angle, respectively. Fig.6 shows the variation of rolling moment coefficient with rolling angle around these positions. At position A, a clockwise lobe in dotted line indicates that the energy shift from the fluid to delta wing, therefore the rolling angle experiences an augmentation of amplitude. At position C, a counter-clockwise lobe in dash line indicates that the energy shift from the delta wing to the fluid. Consequently, the rolling angle experiences an attenuation of amplitude. The situation at position B is more complicated than those at A and C, the hysteresis loop of rolling moment coefficient shows double "8" style. The curve B is constituted of a large inner lobe in clockwise and two small outer lobes in counter-clockwise. The total area of the two outer cycles is nearly identical with that of the inner cycle indicating that the shift of energy achieved a balance between delta wing and fluid.

A widely accepted opinion agrees that the lift force of delta wing can be enhanced by pitching up, but the enforcement of lift force will be significantly weakened when the wing rock takes place during pitching up. As depicted in Fig.7a and Fig.7b, the lift force coefficient of delta wing in force pitching and free rolling is obviously lower than that of the single DOF

pitching up motion denoted by dash line. In Fig.7c and Fig.7d, the side force coefficient and roll moment coefficient of force pitching and free rolling is lager than those of the single DOF pitching up, indicating the degeneration of the transverse stability.

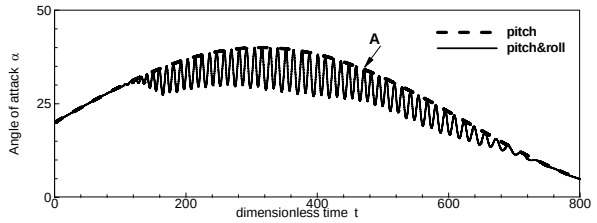

(a) Angle of attack

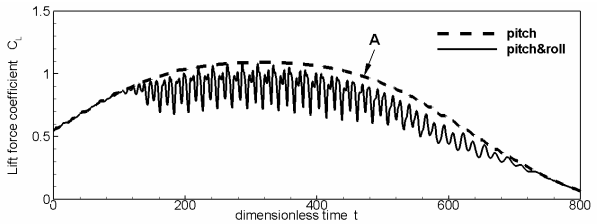

(b) Lift force coefficient

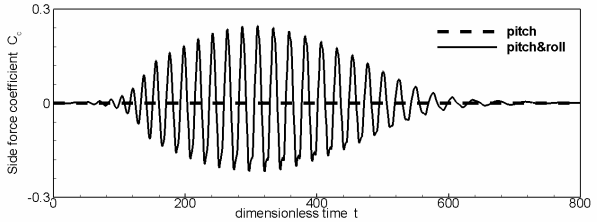

(c) Side force coefficient

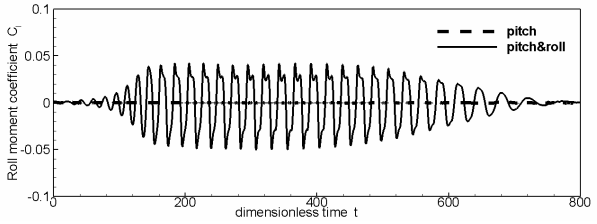

(d) Roll moment coefficient

Fig. 7 Aerodynamics characteristics of delta wing in combined force-pitch and free-roll

C. Sensitive Factors

As was discussed in last section (IV.B) that the double DOF motion in force pitching and free rolling is sensitive to various factors, a numerical investigation about the influence of these factors is conducted, including the roll-axis moment of inertia, structural damping and turbulence flow.

First, the influence of roll-axis moment of inertia is investigated with the same pitching motion in Fig.3 besides the same free-stream conditions. The resultant time histories of delta wings with different roll-axis moment of inertia are compared with that in Fig.3. Fig.8a shows the responses of the delta wings with a larger I_x=1.64. A significant declination of rolling frequency and amplitude are observed. Moreover, the larger onset angle of free rolling motion is observed also. In Fig.8b, with a smaller I_x=0.33, the opposite tendency is achieved, including an earlier onset, and increasing rolling amplitude and frequency. The phenomenon in Fig.8 indicates that roll-axis moment of inertia have great influence on the amplitude, frequency and onset angle of delta wing in force pitching and free rolling.

Computational time histories of delta wing in figure 9 are compared with that in Fig.8a to address the influence of structural damping on the characteristics of delta wing in double DOF motion. In Fig.9, the linear damp is introduced numerically and all other computational conditions are the same. With smaller structural damping coefficient of μ_x=0.033, in Fig.9a, it is observed that the onset angle of free rolling is slightly postponed and the frequency of free rolling is almost coincident with the result without structural damping in Fig.8a. However, the amplitude of free rolling and the movement around zero-incidence are extremely limited. Moreover, in Fig.9b, with larger structural damping coefficient of μ_x=0.065 the amplitude of free rolling motion is almost restricted to the equilibrium angle (ϕ=0°). The phenomena in Fig.9 indicate that the structural damping has overwhelming influence on the rolling amplitude of double DOF motion in combined force-pitch and free-roll.

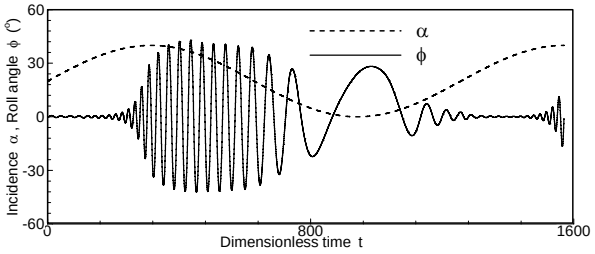

(a) I_x=1.64

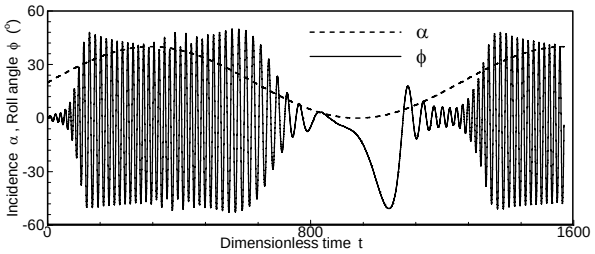

(b) I_x=0.33

Fig.8 The influence of moment of inertia

It is well known that the flow upon delta wing is typically turbulence flow. In order to analyze the influence of turbulence flow, turbulence model is chose as an influence factor of the characteristics of delta wing in combined force-pitch and free-roll. In this section, the Spalart-Allmaras (SA) model is introduced to simulate the turbulence effect of the vortical flow.

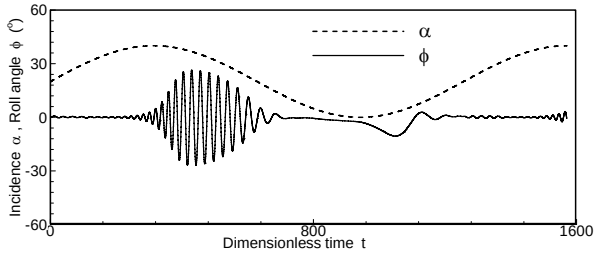

(a) μ_x=0.033

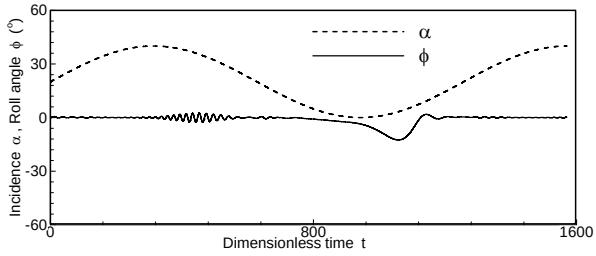

(b) μ_x=0.065

Fig.9 The influence of structural damping coefficient

The computational conditions of Fig.10a are identical with the situation of Fig.3 except the introduction of turbulence model. With the influence of turbulence model, the rapid increase of rolling angle amplitude in upstroke procession of incidence and relatively steady amplitude around the peak of incidence are observed. However, the behavior around the zero incidence of double DOF motion is still obviously different from the experimental data in Fig.4. To understand the issue of discrepancy between computation and experiment, a larger roll-axis moment of inertia, I_x=1.64, is used in the additional computation. A plateau-curve dramatically appears in the trough region of incidence. The behavior around zero incidence of the 80° delta wing in combined force-pitch and free-roll, in Fig.10b, shows a well agreement with experimental result qualitatively. In detail, however, some discrepancies still exist between present calculation and experiment data [17], for example, the transition of the plateau-curve in Fig.10b is smoother than that in Fig.4. This may relate to the influence of the maximum static friction of the bearing, which calls for further investigations. These phenomena in Fig.10 described above indicate that the plateau-curve around zero-incidence is associated with multiple factors, including the roll-axis moment of inertia, turbulence flow and structural damping etc.

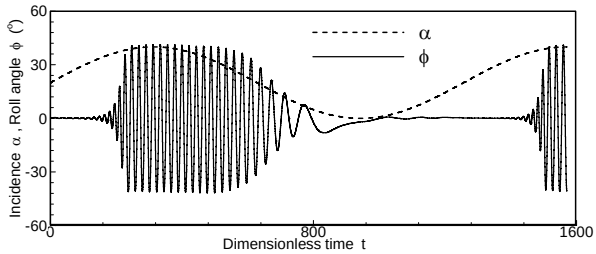

(a) I_x=0.65

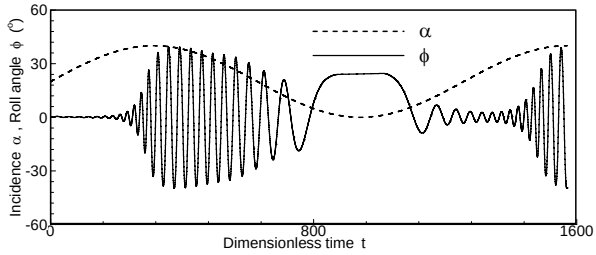

(b) I_x=1.64

Fig.10 The influence of turbulence flow

IV. Conclusions

The unsteady, compressible, full Navier-Stokes equations are integrated time accurately using the implicit, upwind, flux-difference splitting, finite-volume schemes to study the dynamic characteristics of the 80° sharp-edged delta wing in combined force-pitch and free-roll. The wing is forced to oscillate in pitch around an axis located at the half-chord length. The amplitude and reduced frequency of the force motion are 20° and 0.005, respectively. The mean angle of incidence is 20°. The delta wing is released to free roll around the body axis during force pitching. The characteristics of a delta wing in double DOF motion are achieved and qualitatively show a well agreement with experimental data. It has shown that the free-roll motion during forced pitching oscillation significantly decreases the lift force and the transverse stability of delta wing and may lead to severe safety problem. Moreover, the investigation about sensitive factors indicates that the roll-axis moment of inertia and structural damping mainly influence on the frequency and amplitude characteristics of delta wing in combined force-pitch and free-roll, respectively. The plateau-curve in experimental data may be the result of multiple factors, including the roll-axis moment of inertia, turbulence flow, structural damping or more —— a substantial contribution of the CFD to explain some phenomena blended in experiment.

Acknowledgment

The author would like to thank the national academician Zhang Hanxin for his constructive suggestions.

References

[1] R.C. Nelson, A. Pelletier, "The unsteady aerodynamics of slender wings and aircraft undergoing large amplitude maneuvers," Progress in Aerospace Sciences, vol. 39, no.2-3, pp. 185-248. 2003.

[2] L.E. Nguyen, L.P. Yin, and J.R. Chambers, "Selfinduced wing rock of slender delta wing," AIAA paper 81-1883, Aug. 1981.

[3] B.N. Pamadi, D.M. Rao, and T. Niranjana, "Wing rock and roll attractor of delta wing at high angles of attack," AIAA paper 94-0807, 1994.

[4] Ericson, L., "Wing rock analysis of slender delta wings, review and extension," AIAA paper 95-0317, Jan.1995.

[5] X.Z. Huang, and E.S. Hanff, "Non-linear rolling stability of a 65° delta wing model at high incidence," AIAA paper 99-4102, 1999.

[6] N.M. Chaderjian, and L.B. Schiff, "Navier-Stokes prediction of large-amplitude forced and free-to-roll delta-wing oscillations," AIAA paper 94-1884, 1994.

[7] O.A. Kandil, and M.A. Menzies, "Effective control of computationally simulated wing rock in subsonic flow". AIAA paper 97-0831, 1997.

[8] W. Liu, H.X. Zhang, and H.Y. Zhao, "Numerical simulation and physical characteristics analysis for slender wing rock," Journal of Aircraft, vol.43, no.3, pp. 858-861. 2006.
[9] R.M. Hall, and S.H. Woodson, "Introduction to the abrupt wing stall program," Journal of Aircraft, vol.41, no.3, pp. 425-435. 2004.
[10] R.M. Hall, "Introduction: Abrupt Wing Stall program, Part 2," Journal of Aircraft, vol.42, no.3, pp. 577-577. 2005.
[11] R.M. Hall, S.H. Woodson, and J.R. Chambers, "Accomplishments of the Abrupt-Wing-Stall program," Journal of Aircraft, vol.42, no.3, pp. 653-660. 2005.
[12] O.A. Kandil, and H.A. Kandil, "Pitching oscillation of a 65-degree delta wing in transonic vortex-breakdown flow," AIAA paper 94-1426-CP, 1994.
[13] Y.A. Abdelhamid, and O.A. Kandil, "Effect of reduced frequency on super maneuver delta wing," AIAA paper 98-0415, 1998.
[14] C. Jouannet, and P. Krus, "Lift coefficient predictions for delta wing under pitching motions," AIAA paper 2002-2969, 2002.
[15] O.A. Kandil, and M.A. Menzies, "Coupled rolling and pitching oscillation effects on transonic shock-induced vortex-breakdown flow of a delta wing," AIAA paper 96-0828, 1996.
[16] H.J. Kowal, and A.D. Vakili, "An investigation of unsteady vortex flow for a pitching-rolling 70-deg delta wing," AIAA paper98-0416, 1998.
[17] M.Z. Tang, W. Zhang, and H.L. He, "Experimental investigation on unsteady flow field about a coupled pitching-rolling delta wing," Acta Aerodynamica Sinica, vol. 19, no. 1, pp.47-55. 2001.
[18] M.J. Khan, and A. Ahmed, "Response of vortex breakdown induced wing rock to pitching & plunging," AIAA paper 2004-4732, 2004.
[19] J.M. Elzebda, D.T. Mook, and A.H. Nayfeh, "Influence of pitching motion on subsonic wing rock of slender delta wings," Journal of Aircraft, vol. 26, no. 6, pp. 503-508. 1989.
[20] J. Er-El, D. Seter, and D. Weihs, "Nonlinear aerodynamics of a delta wing in combined pitch and roll," Journal of Aircraft, vol. 26, no. 3, pp. 245-259. 1989.
[21] J. Blazek, *COMPUTATIONAL FLUID DYNAMICS: PRINCIPLES AND APPLICATIONS* (Book style). First edition 2001, *ELSEVIER SCIENCE Ltd.* 2001, pp. 16-18.
[22] Q. Shen, and H.X. Zhang, "A new upwind NND scheme for Euler equations and its application to the supersonic flow," in Proceedings of Asia Workshop on CFD, Sichuan, China, 1994.
[23] A. Jameson, "Time dependent calculations using multigrid with application to unsteady flows past airfoils and wings," AIAA paper 91-1596, 1991.